


Article

Mechanical Properties and Energy Evolution Laws of Rocks Under Freeze–Thaw

Xiaopeng Yue ¹, Ting Liu ^{1,2}, Tao Wen ^{1,2,3,4,*} , Wenjun Jia ^{1,2} and Yajuan Wu ¹

- ¹ School of Geosciences, Hubei Key Laboratory of Complex Shale Oil and Gas Geology and Development in Southern China, Yangtze University, Wuhan 430100, China; hr@zpetro.cn (X.Y.); 2024710599@yangtzeu.edu.cn (T.L.); junn.stu@yangtzeu.edu.cn (W.J.); 15290999666@163.com (Y.W.)
- ² International Cooperation Center for Mountain Multi-Disasters Prevention and Engineering Safety, Yangtze University, Wuhan 430100, China
- ³ Jiacha County Branch of Hubei Yangtze University Technology Development Co., Ltd., Shannan 856499, China
- ⁴ Anhui Institute of Intelligent Underground Detection Technology, Hefei 230601, China
- * Correspondence: wentao200840@yangtzeu.edu.cn

Abstract: In high-altitude mountainous areas, the phenomenon of rock frost damage under repeated freeze–thaw cycles are pronounced, with the deformation and failure processes of rock often accompanied by energy dissipation. To elucidate the energy evolution mechanism of rocks under freeze–thaw cycles, triaxial compression tests and numerical simulation tests were conducted under different freeze–thaw cycles. Results from indoor tests indicate that successive freeze–thaw cycles deteriorate the mechanical properties of rocks. Compared to conditions without freeze–thaw cycles, after 40 freeze–thaw cycles, the peak stress of the rock decreased by 42.8%, the elastic modulus decreased by 64%, and, with increasing confining pressure, the rate of decrease lessened, indicating that confining pressure can inhibit the decline in the mechanical properties of rocks. As the freeze–thaw cycles increase, the total absorption energy (TAE) of rocks gradually decreases. Meanwhile, with increasing confining pressure, the TAE, elastic strain energy (ESE) and dissipated energy (DE) of rocks all gradually increase. However, as the confining pressure increases, the TAE increases by 781%, the ESE increases by 449%, and the DE increases by 6381%. Numerical simulation results reveal that with an increase in the freeze–thaw cycles, shear failure phenomena gradually decrease while tensile failure phenomena gradually increase. During the compression process, the evolution of internal cracks in rocks demonstrates a trend of slow–steady–rapid development, with the number of cracks produced being positively correlated with the freeze–thaw cycles. The performance can provide valuable insights into the degradation mechanism of the mechanical properties of rocks and failure analysis in high-altitude mountainous areas.



Academic Editor: Christos S. Akkratos

Received: 19 December 2024

Revised: 20 January 2025

Accepted: 23 January 2025

Published: 26 January 2025

Citation: Yue, X.; Liu, T.; Wen, T.; Jia, W.; Wu, Y. Mechanical Properties and Energy Evolution Laws of Rocks Under Freeze–Thaw. *Water* **2025**, *17*, 353. <https://doi.org/10.3390/w17030353>

Copyright: © 2025 by the authors. Licensee MDPI, Basel, Switzerland. This article is an open access article distributed under the terms and conditions of the Creative Commons Attribution (CC BY) license (<https://creativecommons.org/licenses/by/4.0/>).

Keywords: freeze–thaw cycle; mechanical properties; energy evolution; numerical simulation; crack

1. Introduction

In high-altitude mountainous regions characterized by typical cold climates, the strength of rocks deteriorates under repeated freeze–thaw cycles, exhibiting significant complexity and diversity in the degradation process [1–3]. This degradation involves aspects such as strength reduction, crack propagation, and energy fluctuations, posing a potential threat to the stability of engineering structures [4,5]. Therefore, it is essential to

conduct the influence mechanisms of freeze–thaw cycles on the strength properties of rocks to ensure the stability and safety of major engineering projects.

Considerable progress has been made in the study of the mechanical properties of rocks under freeze–thaw conditions [6–8]. Regarding the effects of freeze–thaw cycles on the physical and mechanical properties of rocks, uniaxial compression tests and acoustic emission tests were conducted under different freeze–thaw cycles to investigate the impact on rocks [9,10]. Results indicate that pore structure expansion caused by water–ice phase change is the primary cause of freeze–thaw damage [11]. In terms of freeze–thaw damage and crack propagation in rocks, a heterogeneous freeze–thaw damage coupled constitutive model was established to vividly describe the initiation, propagation, and coalescence of cracks in rocks under freeze–thaw conditions, highlighting that freeze–thaw damage is an irreversible cumulative process [12–14]. Researchers have also studied the sensitivity of rock damage under different freeze–thaw cycles and confining pressure conditions, identifying deterioration laws in fractured rock mass due to freeze–thaw damage and exploring the relationship between damage and freeze–thaw cycles [15–17]. During the freeze–thaw cycle, the strength of the rock deteriorates, internal cracks increase, and the rock is more prone to failure [18–20]. In terms of energy evolution, uniaxial compression tests under freeze–thaw cycles have shown that with an increase in cycles, the DE/TAE corresponding to the peak stress point exhibits exponential decay [21–23]. In the damage constitutive models under freeze–thaw cycles, an evolutionary equation for rock damage under the coupled action of freeze–thaw and confining pressure has been established based on the Lemaitre strain equivalent hypothesis theory, further revealing the damage and failure laws of rocks [13,15,17]. Moreover, numerical techniques serve as an essential tool for studying the complex mechanical behavior of rocks and provide effective solutions for issues like rock fracturing [24–26]. In conclusion, there is a lack of literature focusing on the comparative analysis of the degradation laws of rock mechanical properties and energy evolution under different freeze–thaw cycles and confining pressure conditions through triaxial compression tests [18,19]. The energy evolution usually involves the conversion of multiple forms of energy, but the mechanisms and proportional relationships between different forms of energy are still not fully understood [27–30]. The freeze–thaw cycle is an important factor affecting the energy evolution of rocks, which can affect the energy storage and release methods of rocks [20,31]. Additionally, there are still shortcomings in the numerical simulation research on rock mechanics under freeze–thaw conditions [32,33].

This study aims to explore the degradation laws of the mechanical properties of cold region sandstone under freeze–thaw conditions. Through conducting indoor tests and numerical simulation tests under varying freeze–thaw cycles and confining pressure conditions, a systematic comparison of stress–strain curves and energy variations will be performed to analyze the influence of freeze–thaw cycles on the mechanical properties of sandstone, including strength and elastic modulus, thereby elucidating the degradation mechanism and energy evolution laws.

2. Experimental Design

The experimental rock sample is a whole sandstone with uniform lithology, fine-grained structure, and no macroscopic visible joints and fissures. Before the experiment, test the porosity, wave velocity, and quality parameters of the rock sample, and select samples with little difference for the experiment. The samples were obtained from a specific region and were prepared as standard cylindrical specimens with a diameter of 5 cm and a height of 10 cm. Before conducting the freeze–thaw tests, the rock samples were dried in a constant temperature box at (105 ± 1) °C for 12 h. After cooling, the dried weight was measured. Subsequently, under a pressure of 0.1 MPa, the rock samples underwent 4 h

of dry pumping and 2 h of wet pumping using a vacuum pump. After completion, the samples were immersed in room temperature water for 12 h to ensure saturation.

After subjecting the rocks to 0, 10, 20, 30, and 40 freeze–thaw cycles, triaxial compression tests were conducted with confining pressures set at 0 MPa, 3 MPa, 6 MPa, 9 MPa, and 12 MPa. The freeze–thaw cycle tests were performed using a TDS-300 freeze–thaw test machine with a freezing temperature of $-20\text{ }^{\circ}\text{C}$ and a thawing temperature of $+20\text{ }^{\circ}\text{C}$, each lasting for 4 h. The temperature of the freeze–thaw cycle was set based on the temperature of the rock sample location. The experimental procedure and method are illustrated in Figure 1.

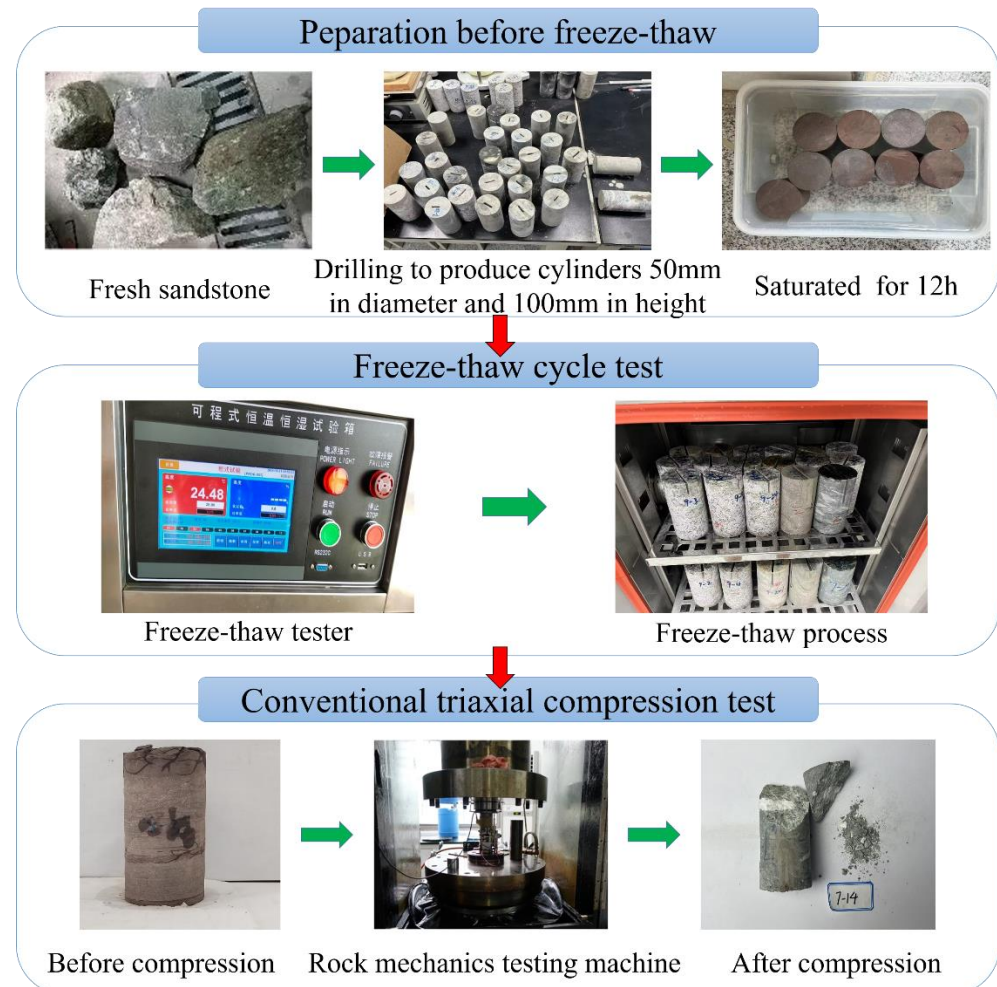


Figure 1. Flowchart of triaxial compression test under freeze–thaw conditions.

3. Experimental Results

3.1. Deterioration Laws of Mechanical Properties

Figure 2 illustrates the stress–strain curves for different freeze–thaw cycles. The rocks generally go through stages of crack closure, elastic deformation, plastic yielding, and failure. With an increase in the freeze–thaw cycles, the peak stress of the rock samples sequentially decreases, while the peak strain slightly increases and the curve slope of the elastic deformation stage gradually decreases. By comparing the initial part of the curve, it is evident that significant deformation occurs under lower stress after freeze–thaw cycles. This indicates that rocks are more prone to deformation after freeze–thaw cycles. As the freeze–thaw cycle increases, this trend becomes more pronounced.

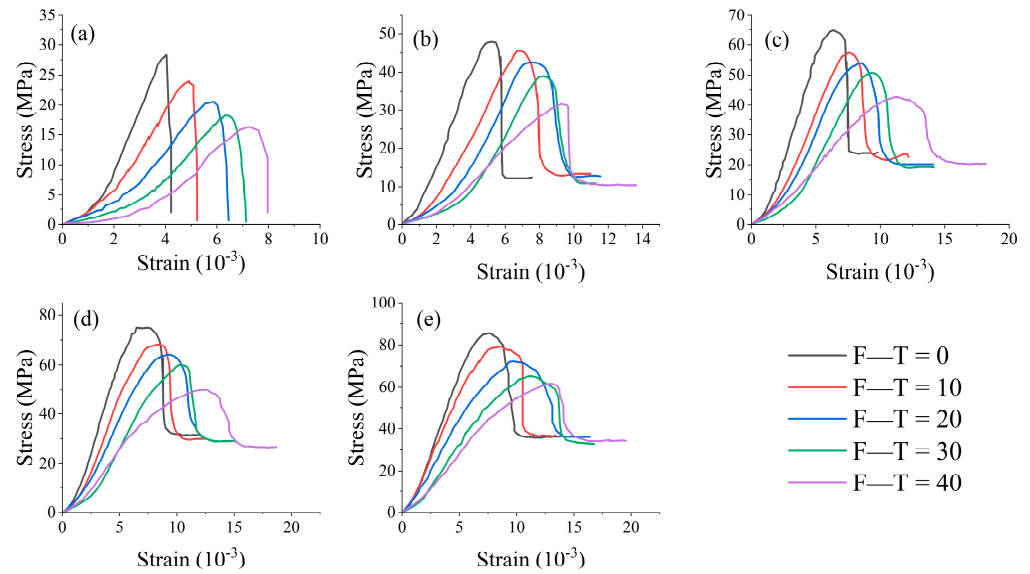


Figure 2. Stress–strain curves under different confining pressures, F-T represents freeze-thaw cycles: (a) 0 MPa; (b) 3 MPa; (c) 6 MPa; (d) 9 MPa; (e) 12 MPa.

To further analyze the influence of freeze–thaw cycles on the mechanical properties of sandstone, the peak stress, peak strain, and elastic modulus under different cycles were determined, as shown in Figure 3. With an increase in the cycles, the peak stress and elastic modulus exhibit a linear decrease overall, while the peak strain shows a linear increase. Taking the curve at a confining pressure of 6 MPa as an example, when the cycles increase to 10, 20, 30, and 40 cycles, the peak stress of the rock samples decreases by 11.51%, 16.80%, 21.74%, and 34.08% compared to 0 cycles, respectively, and the elastic modulus decreases by 28.66%, 37.87%, 47.93%, and 67.56%, respectively. This trend is also observed at other confining pressures. Additionally, under the same freeze–thaw cycles, the elastic modulus increases with increasing confining pressure.

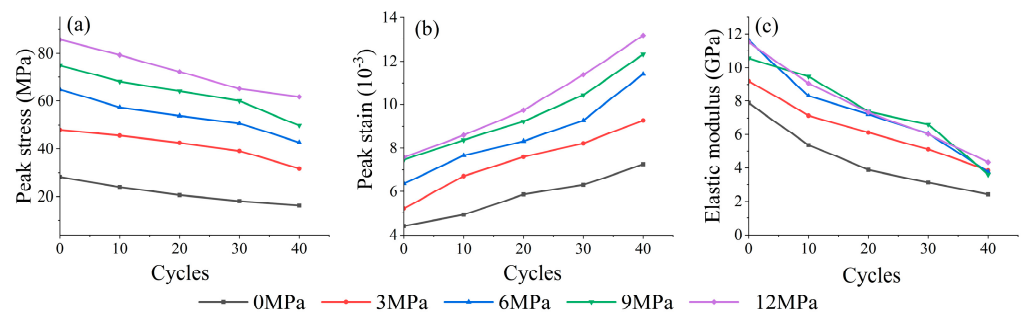


Figure 3. Variation curves of rock strength parameters versus the freeze–thaw cycles: (a) peak stress; (b) peak strain; (c) elastic modulus.

Comparing 40 freeze–thaw cycles with 0 cycles, the decrease in the elastic modulus at various confining pressures exceeds 50%, indicating that freeze–thaw significantly weakens the rock’s deformation resistance. This is due to the frost heave force generated when the pore water freezes into ice during the freeze–thaw cycle process. As shown in Figure 4, the blue region represents water and the yellow region represents ice. The frost heave force leads to the development of internal micropores and microcracks in the rock. Upon thawing, water enters these newly formed micropores and microcracks and further expands the cracks during the next freeze. As the freeze–thaw cycles increase, the phase change during water freezing becomes more thorough, allowing more water to enter the internal micropores and microcracks of the rock, intensifying the damage caused by freeze–thaw

cycles. However, as the freeze–thaw cycle continues to increase, the damage effect becomes less affected by the increasing freeze–thaw cycle due to the sufficient freezing and thawing of water inside the rock.

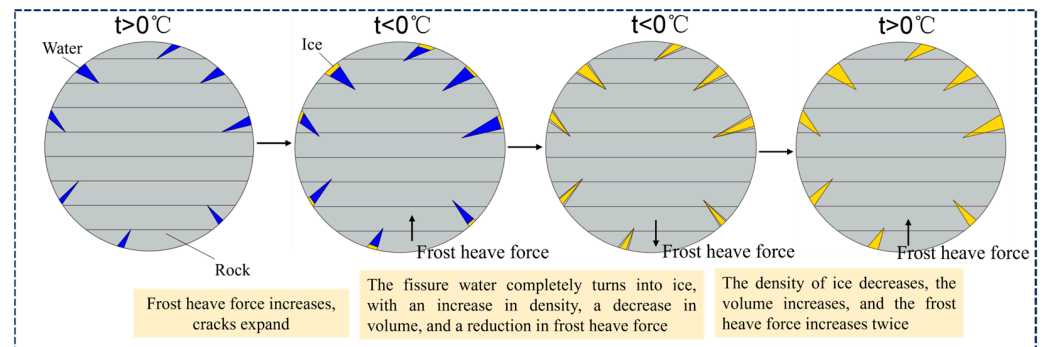


Figure 4. A schematic diagram of the frost heave force model.

Figure 5 illustrates the variation curves of mechanical parameters with the confining pressure. The peak stress and peak strain show a linear relationship with increasing confining pressure. As the confining pressure increases from 0 to 12 MPa, the peak stress of the rock samples after 40 freeze–thaw cycles decreases by 42.8%, 33.8%, 34.1%, 33.4%, and 28.0%, respectively. This indicates that increasing the confining pressure gradually reduces the impact of freeze–thaw cycles on the strength of the rock. Comparing 12 MPa with 0 MPa confining pressures, when the freeze–thaw cycles increase from 0 to 40 cycles, the peak stress increases by 202.1%, 230.4%, 250.1%, 258.9%, and 278.7%, respectively. Therefore, with freeze–thaw cycles increase, the rate of increase in peak stress with increasing confining pressure becomes greater. Overall, with the increase in the confining pressure, the elastic modulus shows an upward trend, indicating that with more freeze–thaw cycles, the impact of confining pressure on the deterioration of rock strength is more significant. However, after a certain number of freeze–thaw cycles, the elastic modulus undergoes significant attenuation, suggesting that freeze–thaw action causes microscopic damage and deterioration inside the rock, weakening its ability to undergo elastic deformation. These microstructural changes require numerical simulation for further analysis.

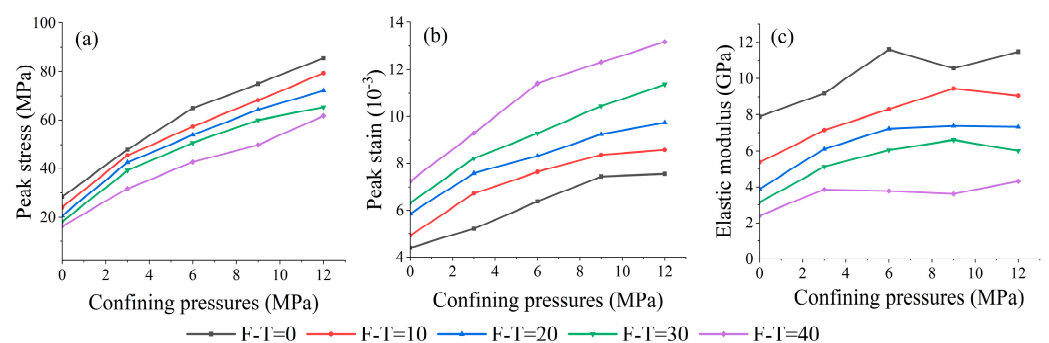


Figure 5. Variation curves of rock strength parameters versus confining pressure: (a) peak stress; (b) peak strain; (c) elastic modulus.

3.2. Energy Evolution Laws

The failure of rocks is closely related to the evolution of energy, where energy dissipation reflects the internal damage of rocks, and energy release drives the rock to undergo failure. Assuming that the rock unit is in a closed system during the deformation and failure process without energy loss through heat exchange or acoustic emission to the external environment, the TAE (U) input by external loads to the rock mass is entirely converted

into releasable ESE (U^e) and the DE (U^d). According to the first law of thermodynamics, the function is expressed as follows [34,35]:

$$U = U^e + U^d \tag{1}$$

When the rock unit is subjected to triaxial principal stress loading, the energy calculation formulas can be expressed as

$$U = \int_0^{E_1} \sigma_1 d\varepsilon_1 + \int_0^{E_2} \sigma_2 d\varepsilon_2 + \int_0^{E_3} \sigma_3 d\varepsilon_3 \tag{2}$$

$$U^e = \frac{1}{2}\sigma_1\varepsilon_1^e + \frac{1}{2}\sigma_2\varepsilon_2^e + \frac{1}{2}\sigma_3\varepsilon_3^e \tag{3}$$

$$\sigma_i^e = \frac{1}{E_i} [\sigma_i - \nu_i(\sigma_j + \sigma_k)] \tag{4}$$

$$U^e = \frac{1}{2E_u} [\sigma_1^2 + \sigma_2^2 + \sigma_3^2 - 2\nu(\sigma_1\sigma_2 + \sigma_2\sigma_3 + \sigma_3\sigma_1)] \tag{5}$$

where σ_i represents the principal stress in the i th direction; σ_i^e denotes the elastic strain corresponding to the three principal stress directions; ν_i signifies the Poisson’s ratio in the three directions; and E_u stands for the unloading elastic modulus. For practical engineering applications, the initial elastic modulus E_0 is often used instead of E_u during calculations.

In conventional triaxial compression, where the second and third principal stresses are equal, the energy calculation formula for the rock can be simplified as follows:

$$U = \int_0^\varepsilon \sigma_1 d\varepsilon_1 + 2 \int_0^\varepsilon \sigma_2 d\varepsilon_2 \tag{6}$$

$$U^e = \frac{1}{2E_u} [\sigma_1^2 + 2\sigma_2^2 - 2\nu(\sigma_1\sigma_2 + \sigma_2^2)] \tag{7}$$

$$U^d = U - U^e \tag{8}$$

Figure 6 illustrates the relationship between rock energy and the freeze–thaw cycles at 0 MPa of confining pressure. As the cycles increase, the TAE of the rock gradually decreases. During the crack closure and elastic deformation stages, internal microcracks in the rock close without significant crack propagation, resulting in relatively low DE. As the rate of internal crack propagation within the rock increases, plastic deformation begins to occur, leading to a gradual increase in DE. Overall, the energy dissipation rate of the rock under different freeze–thaw cycles shows an increasing trend.

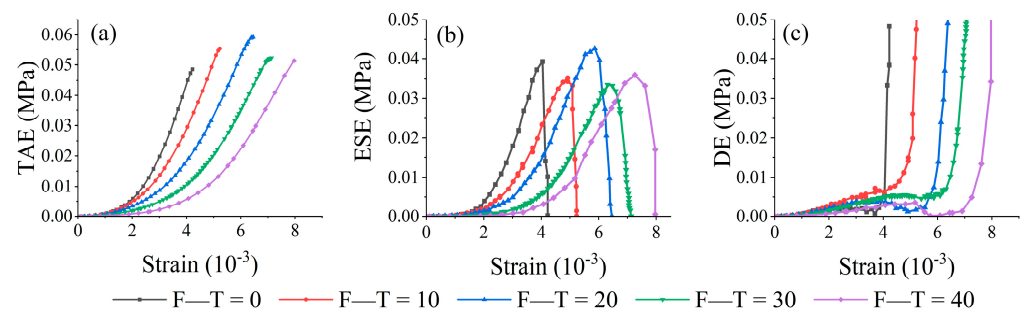


Figure 6. Variation curves of rock energy versus the different freeze–thaw cycles at 0 MPa: (a) TAE; (b) ESE; (c) DE.

Figure 7 displays the relationship between rock energy and confining pressure at 0 freeze–thaw cycles. With increasing confining pressure, the TAE by the rock also gradually

increases. Compared to 0 MPa of confining pressure, the TAE at 3, 6, 9, and 12 MPa of confining pressure increases by 209%, 407%, 674%, and 781%, respectively. The ESE increases by approximately 100%, 208%, 340%, and 449%, while the DE increases by 2041%, 3756%, 6309%, and 6381%. These relationships highlight the impact of freeze–thaw cycles and confining pressure on the energy dynamics of rocks, showcasing how these factors influence energy dissipation and absorption within the rock mass.

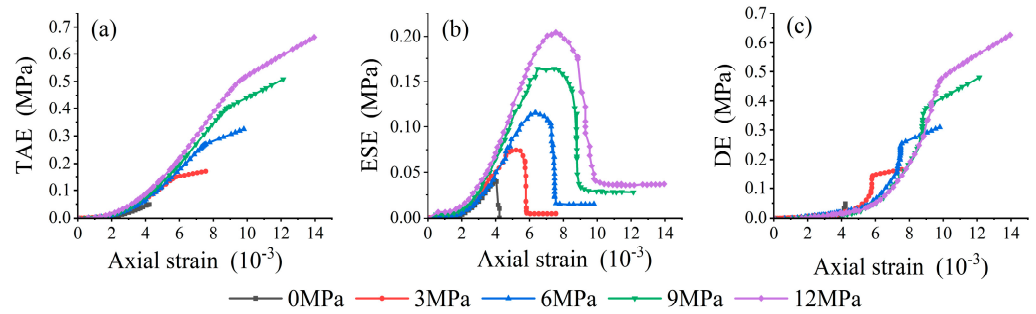


Figure 7. Variation curves of rock energy and confining pressure under 0 freeze–thaw cycle: (a) TAE; (b) ESE; (c) DE.

4. Numerical Simulation

4.1. Numerical Simulation Design

4.1.1. PFC Model Establishment

To further investigate the microstructural failure behavior of rock masses, PFC3D software version 5.0 is employed to simulate the microstructural alterations within the rock masses, helping to reveal the microscopic mechanisms behind the failure behavior of rock masses under macroscopic experimental conditions. A standard model with a diameter of 50 mm and a height of 100 mm is initially constructed, with particle radii randomly distributed between 0.001 and 0.002. The numerical model of the specimen is shown in Figure 8. This model is composed of two materials: rock particles and pore water particles, and its dimensions are consistent with those of the laboratory sample. In the triaxial test simulation, the upper and lower walls represent the loading plates, while the lateral walls are controlled by a servo mechanism to maintain a constant confining pressure throughout the experiment. During the entire compression process, the axial strain, volumetric strain, principal stress, and confining pressure of the sample are continuously recorded.

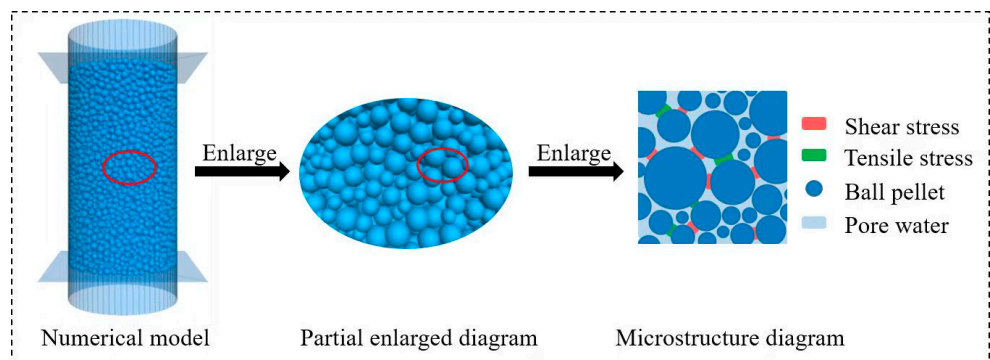


Figure 8. Numerical simulation model.

4.1.2. Microscopic Parameter Calibration

The microscopic parameters of the discrete element particle in the contact mechanics model significantly impact the mechanical properties. In PFC3D simulations, microscopic parameters such as inter-particle friction coefficient, contact stiffness, and initial porosity are

typically calibrated through adjustment parameter methods with macroscopic parameters. Due to the time-consuming nature of adjustment parameter methods, some parameters can be assumed as constant values. For instance, the particle radius is constrained between 0.001 and 0.002, the particle density is set at 2700, and the damping coefficient is set at 0.7. The simulation involves adjusting parameters like elastic modulus, cohesion, and compressive strength to calibrate the microscopic parameters. In numerical simulation, the elastic modulus primarily affects the strain rate of the rock, while the cohesion and the tensile stress influence the peak stress. After multiple trial adjustments, specific values for the microscopic parameters are obtained, as shown in Table 1. It is observed that under the same freeze–thaw cycle, the microscopic parameters of the rock remain consistent, with each parameter decreasing as the freeze–thaw cycles increase. As the freeze–thaw cycles increase, all parameters decrease, indicating the detrimental effect of freeze–thaw conditions on rock deformation and failure.

Table 1. Parameter values under different freeze–thaw cycles.

Freeze–Thaw Cycles	Pb-coh/MPa	Pb-ten/MPa	Pb-fa/°	Fric	Kratio
0	39.6	106.92	77.9	0.3	1.5
10	38	102.6	73.7	0.3	1.5
20	33.3	89.91	70.3	0.3	1.5
30	31.9	86.13	72	0.3	1.5
40	25.2	68.04	71.8	0.3	1.5

4.2. Stress–Strain Analysis

The results of the numerical simulation are depicted in Figure 9. From the graph, it is evident that the results do not capture the rock’s initial crack closure. This discrepancy may arise because, in the PFC3D simulation, the rock is subjected to stress after being already in a densified state, leading directly into the elastic deformation stage. Furthermore, the indoor test results exhibit a more pronounced brittle behavior in the post-peak stage, with a more significant stress drop, while the numerical simulation curve undergoes a more prolonged strain-softening stage after the peak. Consequently, the residual strength obtained from the numerical simulation generally tends to be lower than that observed in indoor tests, while the peak stress remains relatively consistent. Although numerical simulation methods cannot capture the initial compaction stage of rock failure, they can still be used to model the subsequent deformation stages of rock failure.

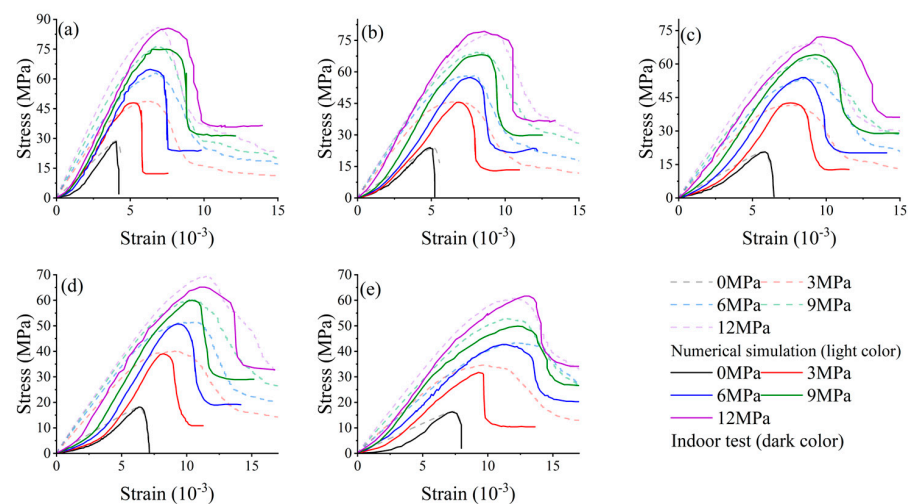


Figure 9. Comparison of stress–strain curves obtained from indoor tests and numerical simulations: (a) 0 MPa; (b) 3 MPa; (c) 6 MPa; (d) 9 MPa; (e) 12 MPa.

4.3. Energy Evolution Law Analysis

Figures 10–12 present the energy evolution laws obtained from numerical simulations at 0, 20, and 40 freeze–thaw cycles. The energy variation laws obtained from numerical simulations is similar to the those obtained from indoor tests. Before reaching the peak stress, both the ESE and the DE increase with axial strain. After the peak stress, the DE continues to rise, while the ESE gradually decreases. This phenomenon occurs because during the post-peak stage, the rapid and extensive propagation of microcracks requires a significant amount of energy, leading to a steep increase in the post-peak DE curve. However, since the numerical simulation essentially lacks the rock’s crack closure stage, the front part of the curves obtained from numerical simulations tends to be steeper compared to those obtained from indoor tests. Additionally, the residual ESE obtained from numerical simulations is generally lower than the ESE observed in indoor tests. Furthermore, the DE eventually tends to approach the TAE.

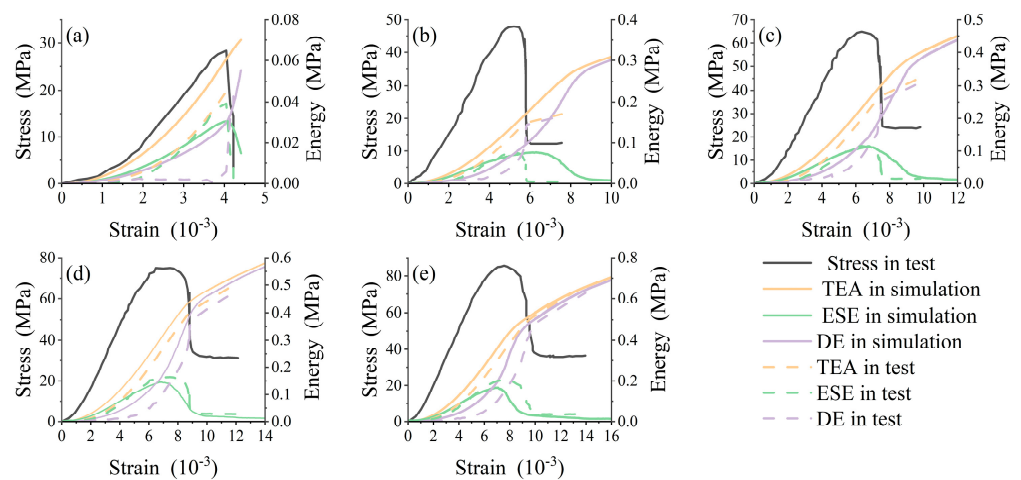


Figure 10. Energy evolution obtained from numerical simulations at 0 freeze–thaw cycles: (a) 0 MPa; (b) 3 MPa; (c) 6 MPa; (d) 9 MPa; (e) 12 MPa.

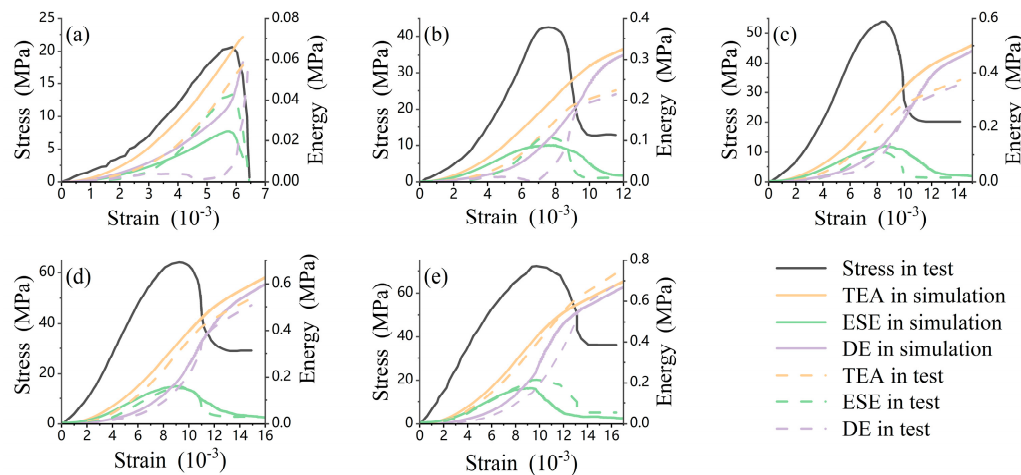


Figure 11. Energy evolution obtained from numerical simulations at 20 freeze–thaw cycles: (a) 0 MPa; (b) 3 MPa; (c) 6 MPa; (d) 9 MPa; (e) 12 MPa.

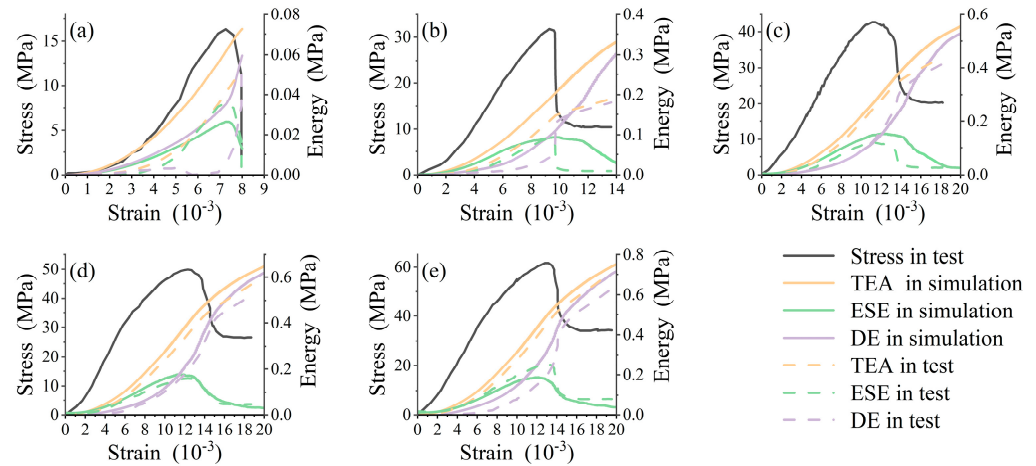


Figure 12. Energy evolution obtained from numerical simulations at 40 freeze–thaw cycles: (a) 0 MPa; (b) 3 MPa; (c) 6 MPa; (d) 9 MPa; (e) 12 MPa.

In the pre-peak stage, especially during the elastic deformation stage, the value of the ESE/TAE is significantly greater than the value of DE/TAE. Numerical simulation results consistently show a much faster and more pronounced increase in the DE compared to indoor test results. However, in the post-peak stage, the DE/TAE remains substantially larger than the ESE/TAE. During the residual deformation stage, the DE/TAE remains relatively constant, while the ESE/TAE gradually decreases and then keeps stable. Furthermore, with an increase in the confining pressure, the TAE, the ESE, and the DE gradually increase. A comparison between the cases of 12 MPa of confining pressure and 0 MPa of confining pressure reveals a decrease in the ESE/TAE corresponding to the peak stress, while the DE/TAE experiences a sharp increase. Consequently, although the ESE increases with rising confining pressure, its proportion diminishes, while the proportion of the DE undergoes a significant escalation.

4.4. Crack Quantity Analysis

The internal deterioration of rocks due to freeze–thaw actions influence their failure characteristics under loading. Therefore, in this section, an analysis is conducted on the relationship between microcracks and the stress–strain curve to evaluate the sample’s fracture process.

4.4.1. Crack Evolution

The stress–strain curve is closely related to crack evolution. Hence, Figure 13 records the curve of cracks evolving with stress–strain changes. The analysis of Figure 13a reveals that during 0 freeze–thaw cycles, cracks mostly appear in the form of shear cracks, with tensile cracks increasing towards the later stages of loading, albeit in much smaller numbers compared to shear cracks. This implies that shear cracks dominate the fracture of the sample during 0 freeze–thaw cycles.

As depicted in Figure 13b–e, with an increase in freeze–thaw cycles, a transition in cracks occurs during sample loading. After 10, 20, 30, and 40 freeze–thaw cycles, the number of shear cracks remains higher than tensile cracks. However, it can be seen from the locally enlarged part of the crack curve that the appearance of tensile cracks is earlier and their quantity gradually increases compared to 0 freeze–thaw cycles. In conclusion, the overall evolution of the crack curve exhibits a trend of slow–steady–rapid development, generally experiencing stages of no cracks (I), crack initiation (II), steady crack propagation (III), accelerated crack propagation (IV), and late-stage crack propagation (V).

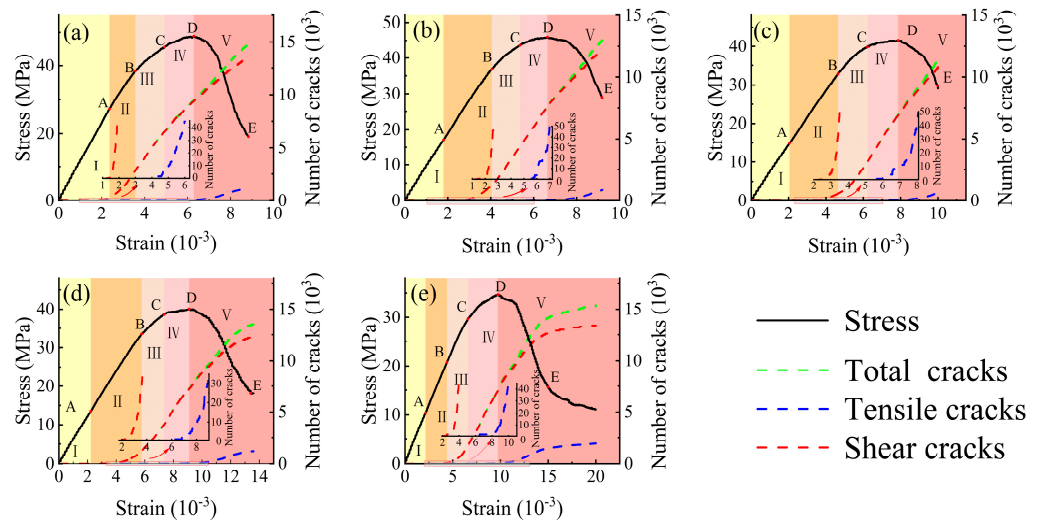


Figure 13. Stress–strain curves and crack evolution: (a) 0 cycles; (b) 10 cycles; (c) 20 cycles; (d) 30 cycles; (e) 40 cycles.

Furthermore, by taking the stress corresponding to the point of initial crack appearance as the initiation stress threshold, the tensile and shear crack initiation stresses and peak stresses after specimen loading are summarized in Table 2. In the 0 MPa of confining pressure, as the cycles increases from 0 to 10, 20, 30, and 40, tensile crack initiation stress decreases by 5.62%, 12.88%, 18.74%, and 33.02%, respectively, while shear crack initiation stress decreases by 10.27%, 18.92%, 27.57%, and 37.84%. This signifies the weakening of interparticle cementation within the rock matrix after some freeze–thaw cycles, where lower stresses during loading can induce crack formation, consequently decreasing load-bearing capacity. During the freeze–thaw cycle processes, moisture within the rock undergoes repeated freezing and thawing. Water expands when freezing, generating expansive forces. These forces exert pressure and dilation effects on the rock’s internal pores, fissures, and structures, leading to the continuous expansion of existing microcracks and the formation of new cracks. Therefore, the integrity of the rock is ultimately destroyed.

Table 2. Crack initiation stress and peak stress under different freeze–thaw cycles.

Freeze–Thaw Cycles	Tensile Crack Initiation Stress/MPa	Shear Crack Initiation Stress/MPa	Peak Stress/MPa
0	42.7	18.5	48.9
10	40.3	16.6	46
20	37.2	15	41.5
30	34.7	13.4	40.7
40	28.6	11.5	34.7

Figure 14 presents the statistical results of the proportion of tensile and shear cracks after loading. Specifically, as the cycles increases to 10, 20, 30, and 40 cycles, the proportion of shear cracks decreases by 5.6%, 11.9%, 16.5%, and 22.1%, respectively, compared to 0 cycles. Conversely, the proportion of tensile cracks increases by 5.6%, 11.9%, 16.5%, and 22.1%, respectively. Furthermore, the ratio of shear cracks to tensile cracks after specimen loading gradually decreases with the increase in cycles, indicating a certain change in the form of microcrack generation after freeze–thaw cycles.

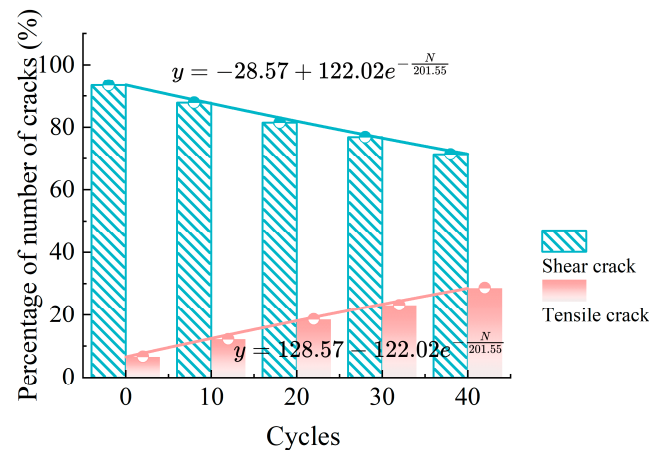


Figure 14. Percentage of the number of cracks under different freeze–thaw cycles.

4.4.2. Fracture Evolution Processes

Taking two specimens, one subjected to 0 freeze–thaw cycles and the other to 40 freeze–thaw cycles, as examples, we investigate the progressive fracture process of sandstone under loading. Figure 15a,b depict the fracture processes of the specimens at various loading stages, where the force chains in the specimens indicate the paths of external load transmission, with the thickness representing the magnitude of the force chain. According to Figure 14, the process of rock fracture evolution is discussed in five stages.

- (a) Stage OA (I): Both the 0-cycle and 40-cycle specimens initially have no cracks. As loading reaches point A, the crack initiation stress of the 30-cycle specimen occurs earlier compared to the 0-cycle specimen, indicating that freeze–thaw action increases the susceptibility to cracking, thereby reducing the load-bearing capacity. Displacement analysis reveals that the 0-cycle and 30-cycle specimens are notably under compression, with the force transmission predominantly being vertical.
- (b) Stage AB (II): This stage marks a slow crack propagation stage. The displacement and force chain analysis of the 0-cycle specimen indicates that at the top and bottom ends, maximum displacement is approximately between 1.5×10^{-4} m and 2.0×10^{-4} m and the maximum force chain value is 1.5×10^3 N. In contrast, the 40-cycle specimen displays that at the ends, maximum displacement is between 3.0×10^{-4} m and 3.5×10^{-4} m and the maximum force chain value is 5.96×10^2 N, suggesting increased deformability under lower loads in the 40-cycle specimen.
- (c) Stage BC (III): During this stage, cracks develop steadily at a faster rate than the stage AB with no significant changes.
- (d) Stage CD (IV): Here, cracks occur rapidly. For the 0-cycle specimen, tensile cracks rapidly aggregate when approaching the peak stress. At a peak stress of 48.9 MPa, the distribution of cracks is at the top of the specimen, as supported by the force chain analysis. Conversely, the 40-cycle specimen behaves distinctly. At a peak stress of 34.7 MPa, clear cracking at the top and bottom occurs in the form of aggregation–expansion–penetration, forming a pronounced fracture zone. Both the 0-cycle and 40-cycle specimens exhibit precursor fracture characteristics near the peak stress.
- (e) Stage DE (V): Entering the post-peak stage, both the 0-cycle and 40-cycle specimens exhibit a steep increase in cracking. When the stress reaches point E, the 0-cycle specimen displays multiple fracture zones along the axis, with a macroscopic fracture zone formed by concentrated cracks. The displacement field shows a downward cone shape. Locally, the force chains indicate residual capacity. In contrast, the 40-cycle specimen at point E shows more prominent macroscopic fracture features, with secondary cracks extending near the fracture zone. The displacement field shifts upward towards

the fracture location, with force chains prominently emphasizing the fractured region. These features collectively indicate that the specimen has been damaged.

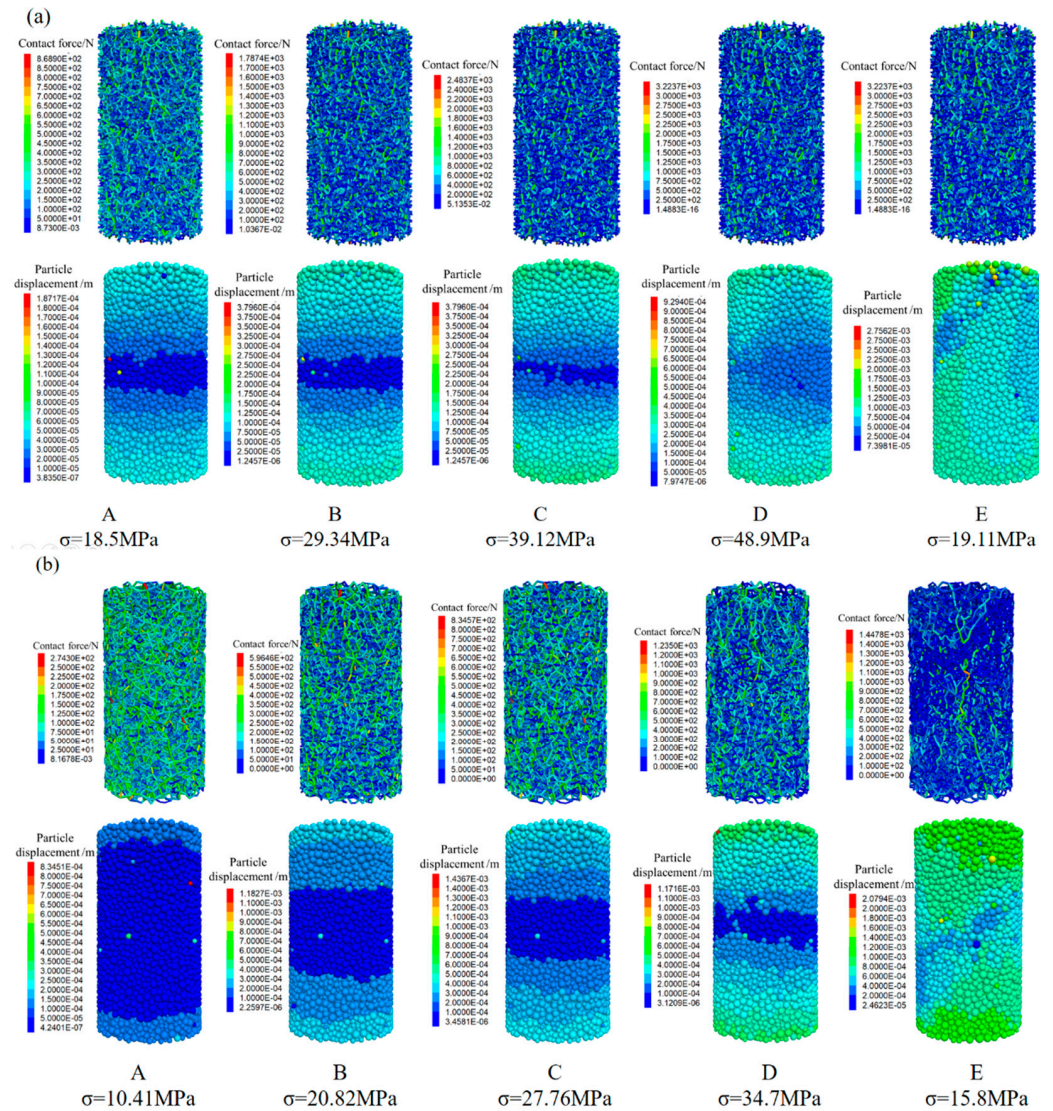


Figure 15. Failure evolution processes under different stages: (a) 0 cycles; (b) 40 cycles.

5. Conclusions

- (1) With 40 freeze–thaw cycles, the peak stress decreased by 42.8%, 33.8%, 34.1%, 33.4%, and 28.0% under different confining pressures compared to 0 cycles. The peak stress and peak strain increase with increasing confining pressure, with a more pronounced yield plateau at higher confining pressures. This indicates that both freeze–thaw and confining pressure lead to the transition of rock from brittle to ductile failure. Additionally, the elastic modulus decreased by 64.0%, 65.1%, 59.3%, 55.5%, and 58.8%, signifying a significant weakening of the rock’s deformation resistance due to freeze–thaw action.
- (2) As the cycles increase, the TAE of the rock gradually decreases. With increasing confining pressure, the TAE, the ESE, and the DE all increase. Compared to 0 MPa of the confining pressure, the TAE at 3, 6, 9, and 12 MPa increases by 209%, 407%, 674%, and 781%, respectively. Furthermore, the ESE increases by approximately 100%, 208%, 340%, and 449% and the DE increases by 2041%, 3756%, 6309%, and 6381%.
- (3) Shear failure is the primary factor leading to rock failure. However, shear failure gradually decreases with an increase in freeze–thaw cycles, with the proportion of

tensile cracks increasing. The cracks generated under loading are the propagation and penetration of microcracks caused by freeze–thaw damage.

- (4) The evolution of cracks during the loading of specimens shows a trend of slow–steady–rapid development. The number of cracks formed during loading is positively correlated with the freeze–thaw cycles, while it is negatively correlated with the tensile and shear crack initiation stresses. As the freeze–thaw cycles increase, the proportion of shear and tensile cracks after loading decreases.

Author Contributions: X.Y.: Methodology, Formal analysis, Investigation, Validation, Writing—original draft. T.L., W.J. and Y.W.: Methodology, Writing—original draft. T.W.: Methodology, Supervision, Project administration, Funding acquisition. All authors have read and agreed to the published version of the manuscript.

Funding: The work was funded by the National Natural Science Foundation of China (No. 42477174); Science and technology program of Tibet Autonomous Region (XZ202301YD0034C, XZ202402ZD0001, XZ202202YD0007C); Open Fund of Anhui Intelligent Underground Detection Technology Research Institute (AHZT2023KF03); Qinghai Province Basic Research Program Project (2024-ZJ-904); the 16th and 17th Innovation and Entrepreneurship Training Program for College Students at Yangtze University.

Data Availability Statement: The datasets generated during and/or analyzed during the current study are available from the corresponding author on reasonable request.

Conflicts of Interest: Author Tao Wen was employed by the company Jiacha County Branch of Hubei Yangtze University Technology Development Co., Ltd. The remaining authors declare that the research was conducted in the absence of any commercial or financial relationships that could be construed as a potential conflict of interest.

References

- Jia, H.L.; Ding, S.; Zi, F.; Dong, Y.H.; Shen, Y.J. Evolution in sandstone pore structures with freeze-thaw cycling and interpretation of damage mechanisms in saturated porous rocks. *Catena* **2020**, *195*, 104915. [\[CrossRef\]](#)
- Sharma, M.; Satyam, N.; Reddy, K.R. Effect of freeze-thaw cycles on engineering properties of biocemented sand under different treatment conditions. *Eng. Geol.* **2021**, *284*, 106022. [\[CrossRef\]](#)
- Zhang, J.B.; Du, R.H.; Zhang, X.H.; Wu, J.; Xiang, X. Experimental and numerical investigation of the rheological characteristics of tunnels in cold regions during excavation and operation. *Acta Geotech.* **2024**, *19*, 1943–1964. [\[CrossRef\]](#)
- Yahaghi, J.; Liu, H.; Chan, A.; Fukuda, D. Experimental and numerical studies on failure behaviours of sandstones subject to freeze-thaw cycles. *Transp. Geotech.* **2021**, *31*, 100655. [\[CrossRef\]](#)
- Zhang, J.; Deng, H.W.; Taheri, A.; Ke, B.; Liu, C.J.; Yang, X.R. Degradation of physical and mechanical properties of sandstone subjected to freeze-thaw cycles and chemical erosion. *Cold Reg. Sci. Technol.* **2018**, *155*, 37–46. [\[CrossRef\]](#)
- Hou, C.; Jin, X.G.; He, J.; Li, H.L. Experimental studies on the pore structure and mechanical properties of anhydrite rock under freeze-thaw cycles. *J. Rock Mech. Geotech. Eng.* **2022**, *14*, 781–797. [\[CrossRef\]](#)
- Momeni, A.; Abdilor, Y.; Khanlari, G.R.; Heidari, M.; Sepahi, A.A. The effect of freeze-thaw cycles on physical and mechanical properties of granitoid hard rocks. *Bull. Eng. Geol. Environ.* **2016**, *75*, 1649–1656. [\[CrossRef\]](#)
- Wang, Y.; Han, J.Q.; Li, C.H. Acoustic emission and CT investigation on fracture evolution of granite containing two flaws subjected to freeze-thaw and cyclic uniaxial increasing-amplitude loading conditions. *Constr. Build. Mater.* **2020**, *260*, 119769. [\[CrossRef\]](#)
- Cao, J.P.; Hu, J.; Wang, X.R.; Yang, B.; Xia, Z.G.; Wang, H.K.; Zhang, L.B. Mechanical properties and acoustic emission characteristics of mixed granite after different numbers of freeze-thaw cycles. *Sci. Rep.* **2024**, *14*, 14074. [\[CrossRef\]](#)
- Shi, C.D.; Nie, W.; Ma, G.W.; He, M.C.; Chen, Y. Effects of freeze-thaw cycles on granite failure using acoustic emission test. *J. Rock Mech. Geotech. Eng.* **2024**. [\[CrossRef\]](#)
- Qiao, C.; Song, Z.Y.; Wang, Y.; Tannant, D.; Li, C.H. Fractures and acoustic emission features of non-persistent jointed rocks subjected to freeze-thaw-compression load: Experimental insights. *Rock Mech. Rock Eng.* **2022**, *55*, 109–123. [\[CrossRef\]](#)
- Huang, S.B.; Liu, Q.S.; Cheng, A.P.; Liu, Y.Z. A statistical damage constitutive model under freeze-thaw and loading for rock and its engineering application. *Cold Reg. Sci. Technol.* **2018**, *145*, 142–150. [\[CrossRef\]](#)
- Lu, Y.N.; Li, X.P.; Chan, A. Damage constitutive model of single flaw sandstone under freeze-thaw and load. *Cold Reg. Sci. Technol.* **2019**, *159*, 20–28. [\[CrossRef\]](#)

14. Zhang, J.B.; Zhang, X.H.; Chen, W.; Huang, Z.; Du, R.H. A constitutive model of freeze-thaw damage to transversely isotropic rock masses and its preliminary application. *Comput. Geotech.* **2022**, *152*, 105056. [[CrossRef](#)]
15. Feng, Q.; Xu, J.S.; Cai, C.X.; Liu, W.W.; Jin, J.C.; Han, W.W.; Qin, Z. Damage constitutive model and meso-failure characteristics of freeze-thaw rock under triaxial compression. *Bull. Eng. Geol. Environ.* **2024**, *83*, 112. [[CrossRef](#)]
16. Jiang, W.T.; Lai, Y.M.; Yu, F.; Ma, Q.G.; Jiang, H.Q. Mechanical properties investigation and damage constitutive models of red sandstone subjected to freeze-thaw cycles. *Cold Reg. Sci. Technol.* **2023**, *207*, 103776. [[CrossRef](#)]
17. Zhai, Y.; Meng, F.D.; Li, Y.B.; Li, Y.; Zhao, R.F.; Zhang, Y.S. Research on dynamic compression failure characteristics and damage constitutive model of sandstone after freeze-thaw cycles. *Eng. Fail. Anal.* **2022**, *140*, 106577. [[CrossRef](#)]
18. Seyed Mousavi, S.Z.; Tavakoli, H.; Moarefvand, P.; Rezaei, M. Assessing the effect of freezing-thawing cycles on the results of the triaxial compressive strength test for calc-schist rock. *Int. J. Rock Mech. Min. Sci.* **2019**, *123*, 104090. [[CrossRef](#)]
19. Wang, S.; Chen, Y.; Ni, J.; Liu, G.; Fernández-Steeger, T.M.; Xu, C. Mechanical characteristics and mechanism of granite subjected to coupling effect of acidic corrosion and freeze-thaw cycles. *J. Earth Sci.* **2021**, *32*, 1202–1211. [[CrossRef](#)]
20. Zhang, H.; Yuan, C.; Yang, G.; Wu, L.; Peng, C.; Ye, W.; Shen, Y.; Moayed, H. A novel constitutive modelling approach measured under simulated freeze-thaw cycles for the rock failure. *Eng. Comput.* **2021**, *37*, 779–792. [[CrossRef](#)]
21. Ma, Q.Y.; Ma, D.D.; Yao, Z.M. Influence of freeze-thaw cycles on dynamic compressive strength and energy distribution of soft rock specimen. *Cold Reg. Sci. Technol.* **2018**, *153*, 10–17. [[CrossRef](#)]
22. Shi, Z.M.; Li, J.T.; Wang, J. Energy evolution and fracture behavior of sandstone under the coupling action of freeze-thaw cycles and fatigue load. *Rock Mech. Rock Eng.* **2023**, *56*, 1321–1341. [[CrossRef](#)]
23. Wang, P.; Xu, J.Y.; Fang, X.Y.; Wang, P.X. Energy dissipation and damage evolution analyses for the dynamic compression failure process of red-sandstone after freeze-thaw cycles. *Eng. Geol.* **2017**, *221*, 104–113. [[CrossRef](#)]
24. Zhang, L.; Ren, T.; Li, X.C.; Tan, L.H. Acoustic emission, damage and cracking evolution of intact coal under compressive loads: Experimental and discrete element modelling. *Eng. Fract. Mech.* **2021**, *252*, 107690. [[CrossRef](#)]
25. Zhou, Y.; Zhao, D.J.; Li, B.; Wang, H.Y.; Tang, Q.Q.; Zhang, Z.Z. Fatigue damage mechanism and deformation behaviour of granite under ultrahigh-frequency cyclic loading conditions. *Rock Mech. Rock Eng.* **2021**, *54*, 4723–4739. [[CrossRef](#)]
26. Zhu, T.T.; Chen, J.X.; Huang, D.; Luo, Y.B.; Li, Y.; Xu, L.F. A DEM-based approach for modeling the damage of rock under freeze-thaw cycles. *Rock Mech. Rock Eng.* **2021**, *54*, 2843–2858. [[CrossRef](#)]
27. Wen, T.; Tang, H.M.; Wang, Y.K. Brittleness evaluation based on the energy evolution throughout the failure process of rocks. *J. Pet. Sci. Eng.* **2020**, *194*, 107361. [[CrossRef](#)]
28. Wen, T.; Tang, H.M.; Wang, Y.K.; Ma, J.W. Evaluation of methods for determining rock brittleness under compression. *J. Nat. Gas Sci. Eng.* **2020**, *78*, 103321.
29. Wen, T.; Wang, Y.K.; Tang, H.M.; Zhang, J.R.; Hu, M.Y. Damage evolution and failure mechanism of red-bed rock under drying–wetting cycles. *Water* **2023**, *15*, 2684. [[CrossRef](#)]
30. Wen, T.; Wang, Y.; Tang, H. Quantitative evaluation of rock brittle property based on energy evolution and its application in Three Gorges Reservoir area. *J. Earth Sci.* **2024**, *35*, 2013–2029. [[CrossRef](#)]
31. Huang, C.; Zhu, C.; Ma, Y.; Aluthgun Hewage, S. Investigating mechanical behaviors of rocks under freeze-thaw cycles using discrete element method. *Rock Mech. Rock Eng.* **2022**, *55*, 7517–7534. [[CrossRef](#)]
32. Xiong, X.; Gao, F.; Zhou, K.; Yang, C.; Li, J. Mechanical Properties and Strength Evolution Model of Sandstone Subjected to Freeze-Thaw Weathering Process: Considering the Confining Pressure Effect. *Mathematics* **2022**, *10*, 3841. [[CrossRef](#)]
33. Wang, L.; Liu, Z.; Han, J.; Zhang, J.; Liu, W. Mechanical properties and strain localization characteristics of gneiss under freeze-thaw cycles. *Eng. Fract. Mech.* **2024**, *298*, 109937. [[CrossRef](#)]
34. Wen, T.; Tang, H.M.; Wang, Y.K.; Ma, J.W.; Fan, Z.Q. Mechanical characteristics and energy evolution laws for red bed rock of Badong Formation under different stress paths. *Adv. Civ. Eng.* **2019**, *2019*, 8529329. [[CrossRef](#)]
35. Wen, T.; Tang, H.M.; Huang, L.; Wang, Y.K.; Ma, J.W. Energy evolution: A new perspective on the failure mechanism of purplish-red mudstones from the Three Gorges Reservoir area, China. *Eng. Geol.* **2020**, *264*, 105350. [[CrossRef](#)]

Disclaimer/Publisher’s Note: The statements, opinions and data contained in all publications are solely those of the individual author(s) and contributor(s) and not of MDPI and/or the editor(s). MDPI and/or the editor(s) disclaim responsibility for any injury to people or property resulting from any ideas, methods, instructions or products referred to in the content.